ELEMENTA
Science of the Anthropocene

Lange, BA, et al. 2023. Snowmelt contribution to Arctic first-year ice ridge mass balance and rapid consolidation during summer melt. *Elem Sci Anth*, 11: 1. DOI: https://doi.org/10.1525/elementa.2022.00037

RESEARCH ARTICLE

Snowmelt contribution to Arctic first-year ice ridge mass balance and rapid consolidation during summer melt

Benjamin A. Lange[1,2,*], Evgenii Salganik[3], Amy Macfarlane[4], Martin Schneebeli[4], Knut Høyland[3], Jessie Gardner[5], Oliver Müller[6], Dmitry V. Divine[1], Doreen Kohlbach[1], Christian Katlein[7], and Mats A. Granskog[1]

Sea ice ridges are one of the most under-sampled and poorly understood components of the Arctic sea ice system. Yet, ridges play a crucial role in the sea ice mass balance and have been identified as ecological hotspots for ice-associated flora and fauna in the Arctic. To better understand the mass balance of sea ice ridges, we drilled and sampled two different first-year ice (FYI) ridges in June–July 2020 during the Multidisciplinary drifting Observatory for the Study of Arctic Climate (MOSAiC). Ice cores were cut into 5 cm sections, melted, then analyzed for salinity and oxygen ($\delta^{18}O$) isotope composition. Combined with isotope data of snow samples, we used a mixing model to quantify the contribution of snow to the consolidated sea ice ridge mass. Our results demonstrate that snow meltwater is important for summer consolidation and overall ice mass balance of FYI ridges during the melt season, representing 6%–11% of total ridged ice mass or an ice thickness equivalent of 0.37–0.53 m. These findings demonstrate that snowmelt contributes to consolidation of FYI ridges and is a mechanism resulting in a relative increase of sea ice volume in summer. This mechanism can also affect the mechanical strength and survivability of ridges, but also contribute to reduction of the habitable space and light levels within FYI ridges. We proposed a combination of two pathways for the transport of snow meltwater and incorporation into ridge keels: percolation downward through the ridge and/or lateral transport from the under-ice meltwater layer. Whether only one pathway or a combination of both pathways is most likely remains unclear based on our observations, warranting further research on ridge morphology.

Keywords: Sea ice mass balance, Oxygen isotopes, Sea ice ridge, Arctic Ocean, Sea ice habitat

1. Introduction

The most pronounced impacts of climate change have been observed in the Arctic with warming four to five times the global average and dramatic changes to the sea ice cover (Pörtner et al., 2019). The Arctic sea ice cover has shifted from a largely multiyear ice (MYI)-dominated system to a seasonal ice cover dominated by first-year ice (FYI), which has coincided with pronounced thinning and volume loss, and a rapidly declining sea ice extent (Kwok, 2018; Stroeve and Notz, 2018). The thinner and weaker seasonal ice cover has resulted in a more mobile ice pack with an increase in the Transpolar Drift speed (Krumpen et al., 2021) and evidence that deformation processes (e.g., ridging) are increasing in this region (Rampal et al., 2011; Itkin et al., 2017).

A comparison between the MYI-dominated region north of Greenland and the FYI-dominated region in the Beaufort Sea showed that pressure ridging is more prevalent in the MYI-dominated regime (Wadhams and Toberg, 2012), suggesting that a shift to a FYI-dominated ice regime will result in a decline in ridging. This decline is perhaps contrary to Rampal et al. (2011) and Itkin et al. (2017), who suggested an increase in dynamics and ridging under thinner Arctic sea ice pack conditions. Regardless of whether the areal coverage of ridges will increase or decrease in the future, a future Arctic Ocean is certain to be dominated by FYI ridges as opposed to MYI ridges (Wadhams and Toberg, 2012). This is an important consideration as MYI and FYI ridges have very different bio-physical properties.

[1] Norwegian Polar Institute, Fram Centre, Tromsø, Norway
[2] Norwegian Geotechnical Institute, Oslo, Norway
[3] Norwegian University of Science and Technology, Trondheim, Norway
[4] WSL Institute for Snow and Avalanche Research SLF, Davos Dorf, Switzerland
[5] UiT The Arctic University of Norway, Tromsø, Norway
[6] University of Bergen, Bergen, Norway
[7] Alfred-Wegener-Institut Helmholtz Zentrum für Polar- und Meeresforschung, Bremerhaven, Germany

* Corresponding author:
Email: blange.sea.ice@gmail.com

MYI and FYI ridges play a crucial role in the sea ice mass balance of the entire Arctic Ocean (Wadhams and Toberg, 2012; Hansen et al., 2013) and are important for the offshore industry, as both ridge types typically represent the maximum design load on offshore structures and can scour the seafloor in coastal regions (Wright and Timco, 2001; Wadhams and Toberg, 2012). MYI ridges, however, are typically wider and more consolidated (i.e., more mass and momentum) and are composed of fresher, harder and stronger ice in comparison to FYI ridges; thus, MYI ridges pose one of the greatest risks to offshore structures and shipping activities throughout the Arctic Ocean (Richter-Menge and Cox, 1985; Timco and Burden, 1997). Furthermore, the difference in physical properties between FYI and MYI ridges will also mean that they will have different effective densities; thus, altimetry-based freeboard measurements and subsequent interpretation of ice thicknesses will likely be different between the two cases.

First-year ice ridges have also been identified as ecological hotspots in the Arctic (Hop and Pavlova, 2008; Lange et al., 2017b; Fernández-Méndez et al., 2018). Ridges have been proposed to serve as a refuge and feeding ground for ice-associated organisms with shifting sea ice habitats and continued disappearance of summer sea ice (Gradinger et al., 2010), primarily as a result of the relatively large voids (i.e., high macro-porosity) which offer additional suitable habitat and shelter from predators. Furthermore, the unconsolidated composition of FYI ridges enhances the scattering of light and results in light levels within the ridge (e.g., available photosynthetically active radiation for algae) that are significantly higher than the adjacent level sea ice (Katlein et al., 2021).

The keel in a FYI ridge consists of an upper consolidated layer and a lower unconsolidated part (often called the rubble) characterized by a higher macro-porosity (i.e., presence of voids). Old ridges on the other hand have been reported to be almost fully consolidated (e.g., Johnston, 2017). The thickness of the consolidated layer in FYI ridges at the end of winter is about 1.5–2 times the surrounding level ice thickness, a process that is well explained by atmospheric cooling combined with the macro-porosity (Leppäranta et al., 1995; Høyland, 2002; Marchenko, 2008). However, the observed degree of consolidation in old ridges cannot be explained by this process, and the transformation from FYI to SYI ridge seems to occur over the summer (Høyland, 2002). Shestov and Marchenko (2016a, 2016b) carried out laboratory experiments and numerical simulations that showed a decreasing salinity inside the unconsolidated part subsequently increasing the freezing point, which allowed for formation of new ice without an external heat flux. The supply of fresh or low saline water is necessary to accelerate this process and may come from a combination of surface melt (snow and ice) and bottom ice melt.

There are few reports from sea ice ridges in the summer. Only Shestov et al. (2018) report summer values. However, the data from late spring (Høyland, 2002) in the Barents Sea and early winter in the Fram Strait (Shestov et al., 2012) show increasing temperatures and a corresponding decreasing salinity over the summer. The temperatures in the unconsolidated part of FYI ridges (rubble) during the winter and spring seasons are isothermal and equal to the freezing point of the ocean water. After the summer consolidation, temperatures in the lower keel increased, and Shestov et al. (2012) reported average values in different years ranging from -1.1°C to -1.4°C which are above the typical freezing point of seawater.

During the Multidisciplinary drifting Observatory for the Study of Arctic Climate (MOSAiC, Nixdorf et al., 2021; Nicolaus et al., 2022) in the last week of June 2020, we observed what appeared to be a FYI ridge keel consolidation event, perhaps surprisingly, during advanced summer melt. Thus, we collected ice cores from two separate ridges to examine meltwater signatures. Supported by snow and ice observations, the data enabled us to determine if the ridges consolidated from meltwater during advanced summer melt, where the meltwater originated (i.e., snow versus sea ice melt), and when the consolidation occurred. These determinations suggest a mechanism that adds a relatively large volume of ice at a time of year when the ice pack is otherwise melting.

2. Materials and methods

2.1. Study site

Here we present observations and samples collected from two FYI ridges within the Central Observatory during leg 4 (June to August 2020), as part of the overall snow and ice sampling and observation program of MOSAiC (Nicolaus et al., 2022). An observatory had been established on one of these ridges, called Alli's ridge, during February 2020 (leg 2). Alli's ridge formed from a lead opening, freezing, then reclosing during a dynamic period from December 7 to December 15, 2019, with block thicknesses of approximately 20–25 cm. Alli's ridge had second year ice (SYI) on one side and FYI on the other side. However, the ridge itself was made primarily of FYI blocks. The second ridge sampled, called Jaridge, formed during a deformation event during February–March 2020 (leg 2). Jaridge also had FYI on one side and SYI on the other side, and consisted primarily of FYI with block thicknesses between 20 and 40 cm (Nicolaus et al., 2022). **Figure 1** shows the location of each ridge site.

2.2. Sea ice and snow sample collection

At each coring site on Jaridge (spacing of 5 m to 17 m between coring sites), we had an extensive physical and biogeochemical coring program consisting of three biological cores (e.g., taxonomy, biomass, particulate organic carbon/nitrogen; not presented here), one temperature core, one salinity/isotope core, and one density core. On July 3, 2020, however, no isotope core was extracted at Jaridge, and thus we only present temperature and salinity data from this coring event. We present results from three additional coring events (July 10, 18 and 24, 2022) at Jaridge including both temperature and salinity/isotope cores. On July 24, 2020, a secondary ice-coring site was located adjacent to Jaridge on the level FYI where we extracted one salinity/isotope ice core to establish the

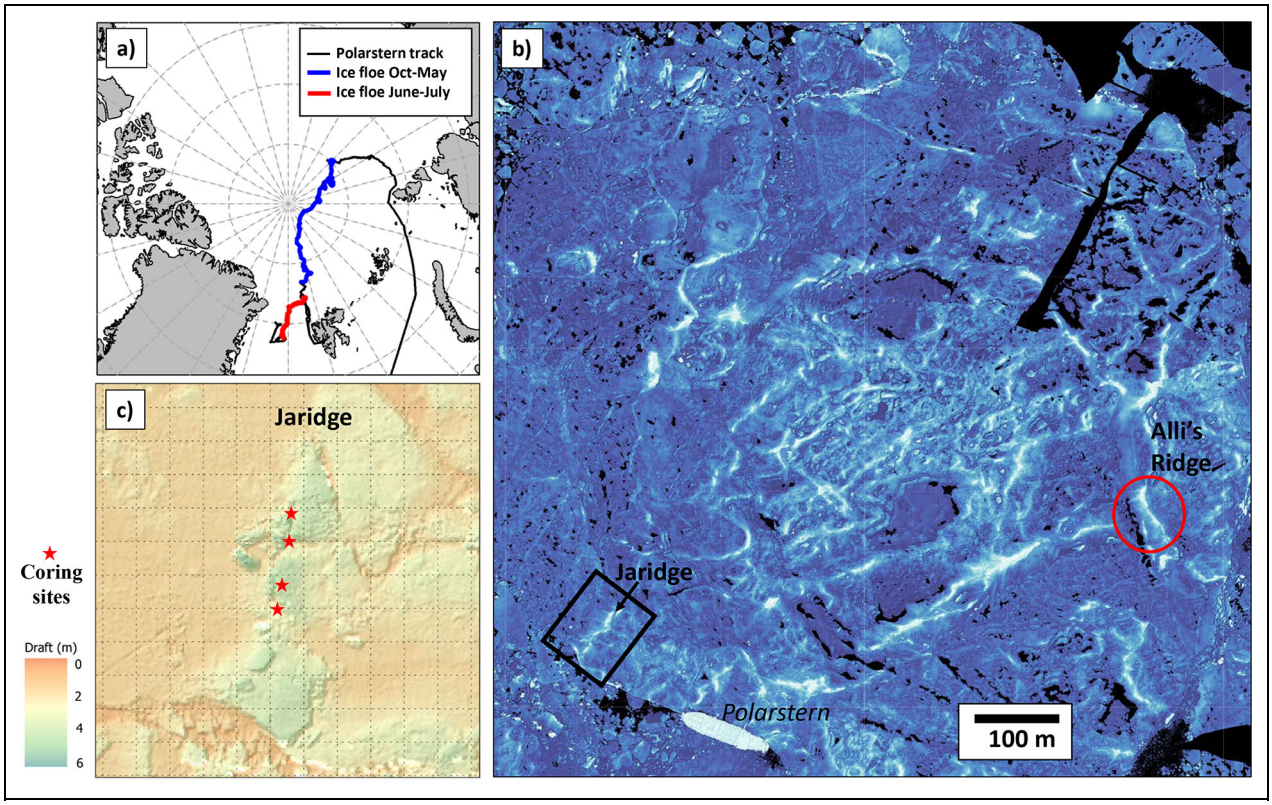

Figure 1. Maps at different scales of the sampling locations. (a) Overview map of the Arctic Ocean with the RV *Polarstern* (Alfred-Wegener-Institut Helmholtz-Zentrum für Polar- und Meeresforschung, 2017) ship track and drift of the MOSAiC ice floe for legs 1 to 3 (blue) and leg 4 (red; drift of the floe between leg 3 and leg 4 is not shown). (b) Airborne laser scanner sea ice or snow surface elevation map (color-scale is approximate freeboard between 0 m and 1.4 m) of the MOSAiC ice floe (conducted on July 17, 2020), also showing the locations of Alli's ridge (red circle) and Jaridge (inside black inset box delineated in panel c; Nicolaus et al., 2022). (c) Multibeam sonar sea ice draft survey (conducted on July 14, 2020) subset centered on Jaridge (inset shown by black square in b), also showing the coring locations (red stars; graticules have 10 m spacing in both dimensions). Core locations are in chronological order starting from the bottom (July 3, 2020) to the top (July 24, 2020).

endmember sea ice values for the mixing model (see below). We also present results from one coring event at Alli's ridge (July 15, 2020), which included temperature and salinity/isotope cores, and salinity measurements from one density core.

Sea ice cores were extracted from the ridges using a 9 cm inner diameter ice corer (Kovacs Enterprise Mark II coring system) powered by a cordless electric drill. The density ice core was extracted using a 7.25 cm internal diameter ice corer (Kovacs Enterprise Mark III coring system). Temperature was measured in situ at 10 cm intervals by first drilling a hole to the center of the ice core with a cordless drill and 4 mm stainless steel drill bit. Immediately after the hole was drilled, the temperature probe (calibrated Testo 720 thermometer) was inserted into the hole and the temperature was recorded once the reading stabilized.

Salinity/isotope ice cores were stored in sterile U-Lines bags (sections <1 m), immediately placed in Styrofoam boxes and transported back to the ship within 2 hours of sampling. Ice cores were stored in a −20°C walk-in freezer until processing. The ice cores were cut into approximate 5 cm sections using a stainless steel, electric butcher band saw. To ensure we captured potential transition zones within the sea ice (i.e., rapid transitions in salinity), we only cut to the top or bottom of natural breaks in the ice cores (i.e., some sections were thicker or thinner than 5 cm but all in the range of 2–7 cm). The samples were placed in plastic cups with lids and melted at room temperature. Once completely melted, approximate 20 ml sub-samples were poured into 20 ml glass or plastic vials with lids and sealed with parafilm for isotope analyses. These samples were stored at 4°C. After the sub-samples were taken, bulk salinity was measured on the remaining water sample using a calibrated YSI 30 conductivity meter (practical salinity scale, unitless).

Snow samples used in this study were collected from sea ice ridges within the Central Observatory during both winter (leg 2, January 2020) and summer (leg 4, June–July 2020). Snow samples were collected using a metal density cutter, melted in the lab in sealed plastic containers and then treated the same as the above ice samples. In our analyses, we used only snow samples collected above a height of 25 cm from the ice surface, as these could be classified as pure snow with no sea ice particles being exchanged through metamorphism at the ice surface. In

total, we included isotopic values from 21 snow samples as the snow endmember values in the mixing model (see below).

2.3. Oxygen isotopic analyses

The stable oxygen isotopic compositions ($\delta^{18}O$) of the melted ice and snow samples were determined in the central laboratory of the Swiss Federal Institute for Forest, Snow and Landscape, Birmensdorf, Switzerland, with an Isotopic Water Analyzer IWA-45-ER (ABB; Los Gatos Research Inc, US). Measurement uncertainty for $\delta^{18}O$ is $\pm$1‰; the precision is $\pm$0.5‰. All samples were measured in duplicate and averaged. The quality control was conducted with three standards for $\delta^{18}O$ at 0.00‰, $-$12.34‰ and $-$55.50‰ and are presented as per mil difference relative to VSMOW (‰, Vienna Standard Mean Ocean Water).

2.4. Mixing model

We quantified the contribution of snow (meteoric origin) to sea ice mass for each sea ice core sample, f_s, using the MixSIAR mixing model (Parnell et al., 2013; Stock et al., 2018) with the source endmember $\delta^{18}O$ ($^{18}O/^{16}O$) signatures of snow and sea ice. The contribution of snow by mass to the entire ice core, F, was calculated by trapezoidal integration and converted to ice depth equivalent (IDE) and snow depth equivalent (SDE) according to Lange et al. (2021), using a snow density of 300 kg m^{-3} and ice density of 900 kg m^{-3}. The mixing model uses tracer data (i.e., isotope ratios) to estimate the proportions of source (i.e., endmember) contributions to a mixture (i.e., ice core sample). Here, we used the Bayesian mixing model, MixSIAR, because it improves upon simpler linear mixing models by taking into account uncertainty within the source endmember values (Parnell et al., 2013; Stock et al., 2018). The Bayesian approach enables us to provide the 95% credible intervals (i.e., confidence intervals in frequentist terms), which means that our estimates for contribution of snow to sea ice mass have a 95% probability of falling within the given range based on the observed data (Parnell et al., 2013; Stock et al., 2018). Values are reported as the mean $\pm$ 95% credible interval.

Here we have two source endmembers, snow and sea ice. The snow endmember values included all snow samples collected at ridges during April–June. The snow endmember samples had a mean $\pm$ one standard deviation (sd) $\delta^{18}O$ ratio of $-$26.8‰ $\pm$ 3.5‰ (n = 33, range: $-$34.6‰ to $-$19.6‰). The sea ice endmember samples had a mean $\pm$ sd $\delta^{18}O$ ratio of $-$0.39‰ $\pm$ 0.47‰ (n = 21, range: $-$1.1‰ to 0.3‰). The sea ice endmembers were taken from a 1.58 m ice core extracted adjacent to Jaridge, because we know that Jaridge formed from this FYI and the surface portion would correspond to the same sea ice during ridge formation and would have experienced similar environmental conditions. We used the same sea ice and snow source endmembers to calculate the snow contribution for the one ice core from Alli's ridge. We assumed that the sea ice had similar values given that the sea ice and ridges formed around the same time and under similar environmental conditions. Furthermore, we assumed that the snow collected from the ridges are representative of snow for each of the sampled ridges given that snow deposition and wind-driven redistribution was likely similar within the small floe.

All data analyses were done with "R" software (R-Development-Core-Team, 2018, v. 3.5.0). The mixing model was implemented using the MixSIAR "R" package (Stock et al., 2018).

3. Results and discussion

3.1. Ridge snow and ice properties

Based on five snow and ice thickness surveys conducted on Jaridge during summer (not presented here), ridge center (i.e., maximum) ice thicknesses ranged between 4.3 m and 7.0 m and maximum snow depth between 0.6 m and 0.75 m. On Alli's ridge during summer, maximum ice thickness ranged between 7.0 m and 8.0 m and maximum snow depth was 0.5 m. Snow depth measurements along the crest (peak) of the ridge indicated thin snow or no snow; however, along the flanks of the ridge and within ice blocks, snow depths were much thicker than on typical level FYI and SYI, which is common for ridges (Liston et al., 2018) and other topographical features (e.g., hummocks, Lange et al., 2017a; Lange et al., 2019). The snow remained longer within and around the ridges than on the surrounding level FYI and SYI.

During the first two snow and ice thickness drilling events on Jaridge (June 25 and July 3, 2020) we observed voids when drilling through the ridge. During the first ice-coring event on July 3, 2020, at Jaridge, we observed voids within the ridge, which are typical features of FYI ridges due to their unconsolidated nature (Høyland, 2002). However, voids were not observed during the later coring events on July 10, 18 and 24, 2020, and were not observed during the remaining drilling events on and after July 4, 2020. This absence of voids is confirmed by the difference in total core length (3.9 m; **Table 1**) and ice thickness (5.4 m; **Table 1**) measured for the temperature core on July 3, 2020, representing a macro-porosity (percentage not sea ice) of 28% (**Table 1**) while the core length and the ice thickness were comparable for all later ice cores extracted from Jaridge, with macro-porosity values of 0% (**Table 1**). The difference in core length and ice thickness for Alli's ridge indicated some void space which, however, only amounted to a macro-porosity of 1% (**Table 1**). The absence of voids was the first indication that consolidation of these voids may have taken place due to the refreezing of meltwater. This phenomenon was the motivation for subsequent salinity/isotope ridge ice cores in order to confirm the consolidation and determine the origin of the meltwater.

Temperature values within all ridge profiles were well below the freezing point of freshwater, indicating that if fresh or relatively fresh, brackish water were to be incorporated or infiltrate the ridge it would freeze (**Figure 2**). Salinity profiles were highly variable, with lowest values near the surface (above sea level) where melt processes and gravitational draining likely had already flushed brine from this sea ice (Cox and Weeks, 1974; Richter-Menge and Cox, 1985). Fresher pockets were also observed in patches

Table 1. Ridge ice core summaries for Jaridge and Alli's ridge

Parameter/Descriptor	Jaridge				Alli's Ridge
Sampling date (2020)	July 3	July 10	July 18	July 24	July 15
Event ID	PS122-4-45_131	PS122-4-46_178	PS122-4-47_199	PS122-4-48_229	PS122-4_47_157
Core length (m)	3.90	4.78	5.92	6.30	5.62
Ice thickness (m)	5.40	4.74	5.94	6.14	6.20
Macro-porosity (%)	28	0	0	0	1
Snow depth (m)	0.52	0.05	0.02–0.17	0.12	0.04
Mean bulk salinity	1.8	2.1	2.8	2.3	2.9
$\delta^{18}O$ (‰) per core section (range)	na[a]	−9.30 to −0.20	−8.64 to 0.90	−5.90 to 0.80	−16.00 to 0.60
Snow fraction by mass (%), f_s, section values (range)	na	2.5–25.4	1.9–29.3	2.0–17.7	2.0–55.7
Snow fraction by mass (%), f_s, below water level (range)	na	2.5–25.4	1.9–18.4	2.4–17.7	2.0–18.7
Snow fraction by mass (%), F, core-integrated mean ± sd (n) [95% credible interval]	na	11.2 ± 4.9 (101) [3.2–21.8]	6.4 ± 3.8 (122) [0.9–15.1]	5.6 ± 3.4 (130) [0.8–13.6]	7.5 ± 3.8 (117) [2.2–16.5]
Ice depth equivalent (m)	na	0.54	0.38	0.35	0.42
Snow depth equivalent (m)	na	1.62	1.14	1.05	1.26

[a] Not available.

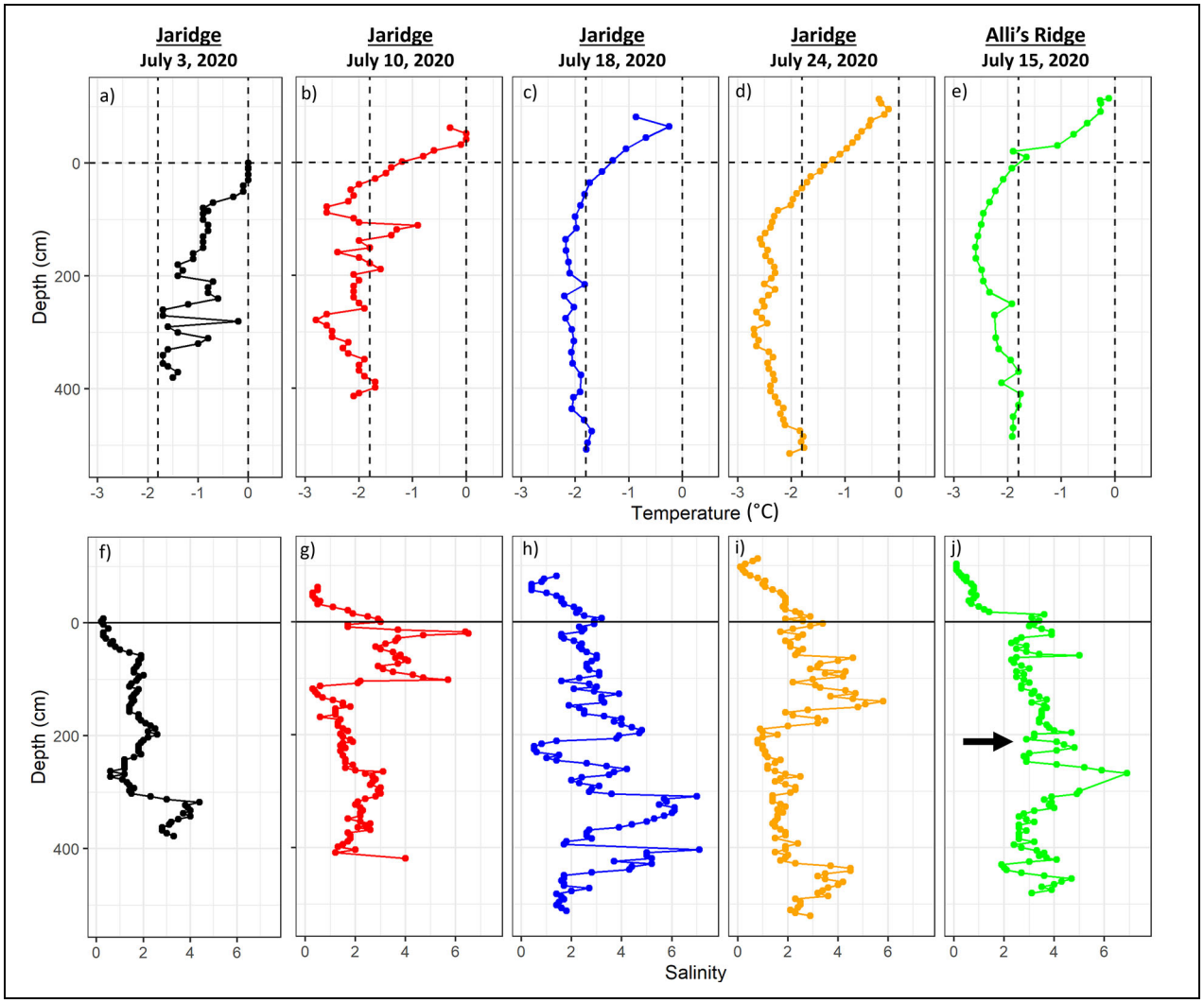

Figure 2. Vertical temperature and salinity profiles of the ridges. (a–e) Profiles of temperature and (f–j) bulk salinity for Jaridge and Alli's ridge ice cores. Dashed vertical lines in (a–e) indicate the freezing temperatures of seawater and freshwater. The dashed (a–e) and solid (f–j) horizontal lines indicate the water line. The black arrow (j) indicates the location corresponding to the black arrow in **Figure 3** and red circle in **Figure 4a**.

at some locations within the ridge profiles, but these were typically below 1–2 m water depth (**Figure 2**).

The variability in salinity of both Jaridge and Alli's ridge (**Figure 2**) were similar to that found in a pressure ridge sampled by Shestov et al. (2018) in June 2015 north of Svalbard, which they assumed to be composed of FYI and named R4. Overall, however, R4 was more saline with peaks up to 10 and only one value slightly lower than 2. Whereas Jaridge had quite many sections with salinity under 2 and maximum values of up to 7 (**Figure 2**). Alli's ridge was perhaps more comparable to R4 (Shestov et al., 2018) but also had salinity values with maxima around 7 (**Figure 2**). The temperature profiles on the first two coring events on July 3 and 10, 2020 (**Figure 2**) were more variable than those reported for R4 (Shestov et al., 2018), however, the shape of the profiles and absolute temperature values for Jaridge (**Figure 2**) were similar to R4 (Shestov et al., 2018). The R4 (Shestov et al., 2018) ridge was sampled in a similar region of the Arctic Ocean, however, nearly one month earlier but still shows some similarities. This could be an indication of the survivability and resilience of sea ice ridges.

Based on salinity alone, it can be inferred that relatively fresh meltwater likely infiltrated the ridge given the very low salinities (<2) in many locations throughout the profiles. However, quantifying how much freshwater these low salinities represent is difficult, because the source salinities are highly variable and a mixing model approach with salinity source values would not yield accurate estimates. Furthermore, the actual source of the meltwater cannot be differentiated from salinity even if source salinities were known. Thus, isotopic analyses were conducted in order to address these questions.

The snow endmember $\delta^{18}O$ value of $-26.8‰ \pm 3.5‰$ is comparable to values reported for Canadian Forces Station Alert, Nunavut, in the Canadian High Arctic, with an annual average snow precipitation value of $-29.7‰$ (Kopec et al., 2016; Lange et al., 2021). In the Eurasian sector of the Arctic Ocean, higher snow precipitation $\delta^{18}O$ values of $-16.8‰ \pm 2.4‰$ have been reported and used

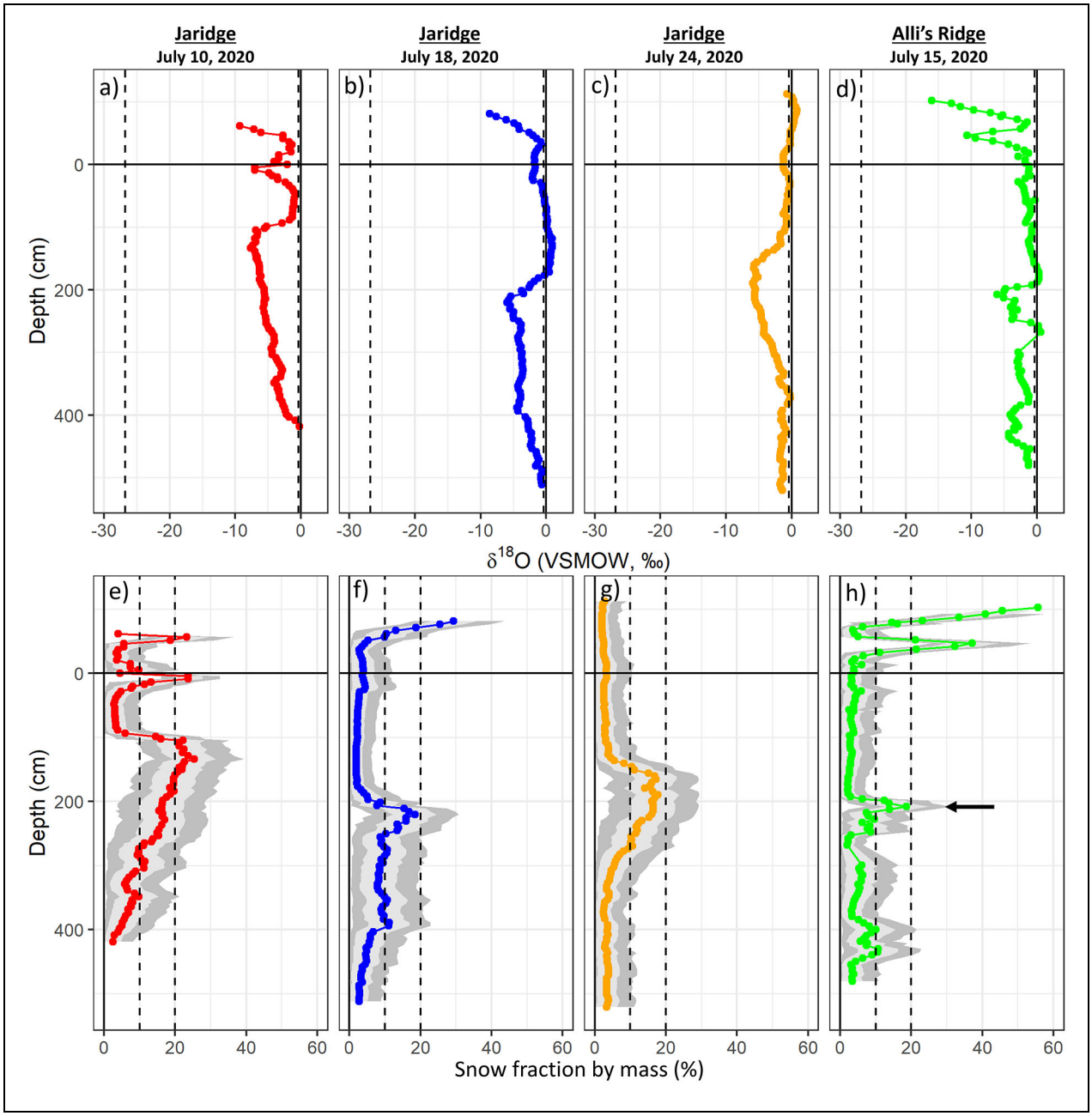

Figure 3. Vertical $\delta^{18}O$ and snow contribution profiles for the ridges. (a–d) Profiles of $\delta^{18}O$ (‰) and (e–h) snow fraction by mass (%) from Jaridge and Alli's ridge ice cores. Dashed vertical lines in the upper panel correspond to the mean snow and sea ice endmember values. In the lower panels, dark grey shading represents 95% credible intervals, and the inner lighter grey shading represents the posterior standard deviation. Dashed lines correspond to 10% and 20% to aid comparison between profiles. The horizontal lines at 0 depth indicate the water level. The black arrow refers to the same feature as in **Figure 2j** and likely similar location in **Figure 4a** (red circle).

for mixing models (Granskog et al., 2017). Variability of the snow $\delta^{18}O$ values and origin are beyond the scope of this study. Nevertheless, we used the $\delta^{18}O$ values from the actual snow found on site as the endmember. Furthermore, the snow samples taken from the ridges had relatively low variability and significantly different isotopic values from sea ice, which is important for accurate estimates of the contribution of snow to the sea ice mass (Stock et al., 2018). The sea ice endmember $\delta^{18}O$ value of $-0.39‰ \pm 0.47‰$ is comparable to sea ice source values of $-0.33‰ \pm 0.23‰$, used for both FYI and MYI from the Lincoln Sea (Lange et al., 2021), and 0‰ for MYI in the Beaufort Sea (Tian et al., 2018), and slightly lower than sea ice endmember values of $2.0 \pm 2.3‰$ reported for FYI and SYI north of Svalbard during the N-ICE2015 campaign (Granskog et al., 2017).

The $\delta^{18}O$ signal of the sea ice section samples was substantially less variable in comparison to the salinity profiles (**Figures 2** and **3**). Overall, core section $\delta^{18}O$ values ranged between $-16.00‰$ and 0.90‰ with core minimum values between $-16.00‰$ and $-5.90‰$ (**Table 1**). These low values provide the first indication

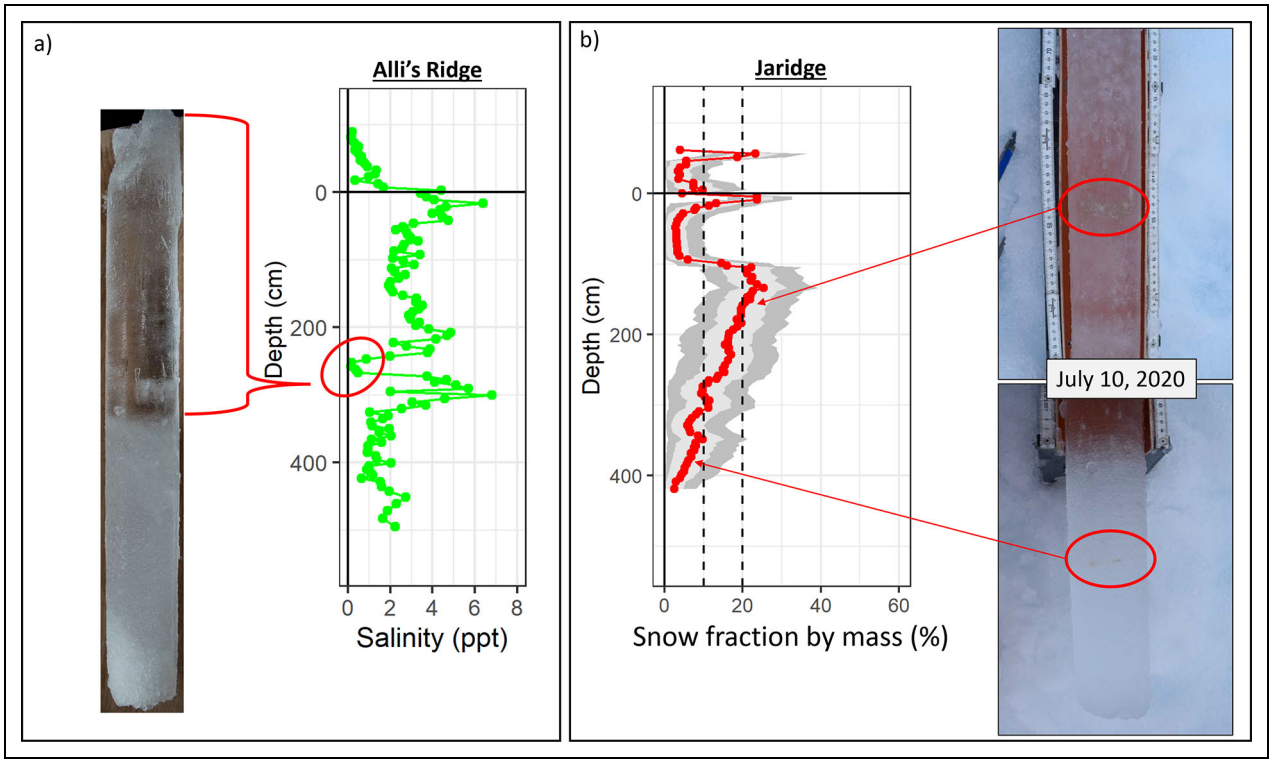

Figure 4. Vertical salinity and percent snow profiles with corresponding photographs. (a) Salinity profile from a 7 cm density ice core (extracted July 15, 2020) at Alli's ridge, with a photograph of the ice core section showing nearly completely fresh, transparent ice in the top portion and the coincident salinity sections delineated by red line and circle. The red circle also delineates a likely similar section of the profiles from **Figures 2j** and **3h** depicted by black arrows. (b) Snow fraction, f_s, profile (July 10, 2020) at Jaridge, with photographs of ice core sections showing where algal aggregates were observed in the ice and the corresponding depths of the algae (red circles and arrows).

that there was substantial meltwater of meteoric origin (i.e., snow) within the sea ice ridges. Using the mixing model with $\delta^{18}O$ data, we can make more accurate estimates of the snow contribution to ice mass within each ridge ice core section and integrated profile.

3.2. Contribution of snow meltwater to ice mass balance

The contribution of snow to the integrated ridge ice core mass, ***F***, was from 5.6% to 11.2% for Jaridge and 7.5% for Alli's ridge (**Table 1**). These estimates of snow contribution fraction for the ridges are higher than previously reported estimates for level Arctic FYI at 3.9% from north of Svalbard prior to melt onset (Granskog et al., 2017) and 4% from the Lincoln Sea in spring (Lange et al., 2021). Our snow contribution estimates are similar to those reported for level SYI at 14.5% (Granskog et al., 2017) and for MYI at 10% ± 5% (Lange et al., 2021). Tian et al. (2018) showed meteoric percentages between 5% and 30% for autumn MYI ice cores from the Beaufort Sea. However, these Beaufort Sea MYI cores were mostly from thin (<70 cm) topographical depressions representing refrozen melt ponds and thus the meteoric signal comes primarily from the melt pond water, which is composed largely of snow meltwater, implying that the total spatially averaged contribution to ice mass balance should be lower.

If we consider the total ice mass, accounting for ice thickness, and convert it to snow depth equivalent, the result is a better representation of the magnitude and overall contribution to ridge ice mass balance. SDE values for Jaridge ice cores ranged from 1.1 m to 1.6 m with 1.3 m for Alli's ridge (**Table 1**). From earlier studies in the Arctic Ocean, but not for level ice only, average SDE estimates were between 0.14 m and 0.16 m for FYI (Granskog et al., 2017; Lange et al., 2021), 0.57 m for SYI (Granskog et al., 2017), 0.8 m for springtime MYI (Lange et al., 2021), and 0.42 m for autumn MYI (Tian et al., 2018). Itkin et al. (2023) reported the average snow depth of 0.14 m for level ice and 0.6 m for large ridges based on Magnaprobe measurements along Central Observatory transects (Nicolaus et al., 2022). The difference between our SDE estimates and the average snow depths on level ice and ridged ice indicates that the snow must have accumulated over a larger area.

The vertical profiles of fraction of snow by mass in the ice core sections, $\boldsymbol{f_s}$, demonstrate some interesting patterns of where snow meltwater was likely incorporated within the ridge (**Figure 3**). There are peaks of high snow contribution within the surface ridge sail (i.e., above water level) of three ice cores (**Figure 3**), which likely resulted from snow entrapped between blocks, the formation of snow-ice, superimposed ice, and/or the formation of hard snow layers not easily distinguishable from ice. Starting within the ridge sail, slightly above or below the water level, are uniform sections of low snow contribution, which were consolidated thermodynamically during

winter (**Figure 3**). Below this layer, starting at 1–2 m water depth, there are peaks of high snow contribution, which extend relatively deeply into the ridge keel for all Jaridge cores (**Figure 3**). Peaks within Alli's ridge, however, are relatively thinner, but a second peak is observed near the bottom of the profile (**Figure 3**). These peaks within the ridge keel have local maxima of snow contribution between 18% and 25% for Jaridge and 19% for Alli's ridge (**Table 1**). If we assume that the 28% macro-porosity of Jaridge is representative of the macro-porosity of the other Jaridge and Alli's ridge coring locations before summer consolidation, then we can estimate how much of the void space was filled with snow meltwater. Void space before summer consolidation would range between 1.34 m and 1.76 m based on a 28% macro-porosity. The IDE estimates of 0.35 m to 0.54 m would result in 20% to 40% of these voids being filled with pure snow meltwater, which agrees well with the snow contribution for core sections of 18% to 25%. Thus, the remainder 60% to 80% of the pre-consolidated void space is likely a combination of seawater and sea ice meltwater; however, being the first observation of such a consolidation event, such mechanisms and thermodynamics require validation through models and additional observations. Nevertheless, our estimates represent a substantial fraction of the ice mass coming from snow meltwater. Similar or even larger peak snow contribution sections were observed in springtime MYI within the Lincoln Sea (Lange et al., 2021); however, these peaks were typically thinner than the high snow contribution layers observed within Jaridge and Alli's ridge. Lange et al. (2021) also observed thicker layers with high snow contribution within the 1 m surface layer of a few ice cores, which represented refrozen melt ponds, superimposed ice and interposed ice.

Large aggregates of ice algae were observed visibly by eye within the ice core on July 10, 2020, at Jaridge (**Figure 4b**). Furthermore, a clear freshwater layer was observed within Alli's ridge (**Figure 4a**), but no $\delta^{18}O$ samples were taken from this 7 cm density core. The adjacent core shows some similarity, but the salinity (black arrows in **Figures 2j** and **3h**) is not nearly as low and the corresponding $\delta^{18}O$ values are not as low as would be expected given the clarity and low, near-zero salinity of the adjacent density core (red circle in **Figure 4a**). This comparison emphasizes the high spatial variability of ridge cores, which is even greater than for level sea ice. Nevertheless, our observations of the fraction of snow contribution showed some consistent patterns with local peaks (i.e., bulges) within the ridge keels, both within the same ridge, Jaridge, and between the two separate ridges, Jaridge and Alli's ridge (**Figure 3**). The surface "winter consolidated" layer also showed relatively uniform and consistently low snow contribution for all ice cores from both ridges (**Figure 3**).

3.3. Mechanism and period of snow meltwater infiltration

How and when this snow was incorporated into the ridges are interesting and complicated questions because different mechanisms may result in the incorporation of snow into a ridge. During ridge formation, snow already present on the surface of the sea ice or snow already incorporated within the sea ice may be incorporated into the ridge as it forms from broken up sea ice blocks. If this were the case, we would expect a more varying and patchy distribution of snow contribution within parts or the entire ice core profile. If the snow on the surface were entrapped in voids or gaps, it would likely remain in them and either remain in liquid form or refreeze in place with no mechanism to flow within the cold, winter sea ice during the period of ridge formation. Snow contributions within FYI, SYI and MYI have a patchy vertical distribution with small peaks either at the surface for FYI or anywhere within MYI (Granskog et al., 2017; Lange et al., 2021). Thus, if any of these ice types were incorporated into the Jaridge or Alli's ridge the percentage contribution of snow within the vertical profile would have also been patchy. Indeed, the ridge profiles of snow contribution show some variability in the surface; however, below the water level the contribution of snow shows gradual transitions or gradients. The relatively larger peaks within the ridge snow contribution profiles have thicknesses that are either thicker than FYI or SYI, or have thicknesses or patterns that have not been observed previously in SYI or MYI (Granskog et al., 2017; Lange et al., 2021).

If the snow was incorporated during the ridge formation event, we would expect to see the signal from the snow within the entire profile; however, in each ridge profile there is an approximate 0.75 m to 2.0 m portion starting near the water level, which has near-zero percent snow contribution (**Figure 4**). This region of the ridge would have also been formed from the same sea ice blocks as the sail above and keel below. This 0.75–2.0 m layer corresponds to the location and approximate thickness of the thermodynamically consolidated layer of FYI ridges, which formed in winter. The consolidated layer gradually thickens after ridge formation due to thermodynamic processes and typically reaches a thickness that can be estimated as approximately 1.5 times the adjacent level ice during winter (Timco and Burden, 1997; Høyland, 2002). The absence of snow contribution in the winter consolidated layer indicates that the incorporation of snow meltwater into the ridge ice must have occurred after the ridge formation, consolidation and freezing period, suggesting that the incorporation of snow into the ridge occurred sometime during the summer melt period. This suggestion is further supported by observations of sea ice algal aggregates within the ridge ice in regions of relatively clear, fresh ice, which also correspond to regions with relatively high percentage snow contribution (**Figure 4**). We find that the presence of algal aggregates within the ice can only be explained by refreezing of water after the onset of algal growth in spring (May), because these large algal aggregates could not have grown within the consolidated ice with its low porosity preventing the supply of sufficient nutrients.

Given the evidence that the incorporation and infiltration of snow into the ridge ice occurred during summer, this incorporation is highly likely to have occurred due to the melting of snow and infiltration into micro- and/or

macro-pores of the ridge ice. Snow meltwater could have infiltrated the ice through lateral movement of freshwater coming from the under-ice freshwater layer present during the sampling period (Smith et al., 2022). Meltwater layers under level ice can contribute to the formation of new ice layers at the interface of meltwater and seawater (e.g., false bottoms), which can delay melt of thinner level ice (Salganik et al., 2023). Usually, the thickness of false bottoms does not exceed 10–15 cm (Eicken et al., 2002). Snow meltwater could have also infiltrated the ridge ice by gravitational forces (isostatic equilibrium) of snow meltwater accumulating above the water level on the surface of the ridge. We cannot say definitively which mechanism drives this process; however, we can conclude that the presence of snow meltwater deep within the ridge keel, even below the depth of the freshwater layer adjacent to the ridge at an approximate 2 m water depth (Smith et al., 2022), demonstrates that the lateral movement alone could not explain snow meltwater infiltrating at depths below 2 m. Rather more likely is that the gravitational isostatic equilibrium of snow meltwater accumulating within the ridge sail percolated down through the ridge, which can then explain the presence of snow meltwater within the deeper regions of the keel below 2 m water depth. There was large spatial variability in the sail height and keel depths at Jaridge ice core sampling locations and also between the ridge sampling locations. This spatial variability is further complicated by a superimposed temporal dimension of 1 week between the sampling events. The large spatial variability in both surface and bottom ice properties likely plays an important role in driving meltwater flow (vertical and horizontal), whether it be above the sea ice and through the micro- and macropore space of the ridge, from adjacent level ice or through under-ice flow of currents and incorporation from below. We note a combination of both mechanisms is possible and that our observations are limited in both spatial extent and temporal coverage in describing the complete mechanisms and flow of snow meltwater to the ridge keel. Modelling and further investigations are needed to better understand the processes of snow meltwater infiltration within ridges and subsequent consolidation.

3.4. Pan-Arctic implications

Shestov and Marchenko (2016a) have demonstrated in a laboratory setting that thermodynamic consolidation of ridges can be the result of meltwater infiltration from below (e.g., keel melt). The conditions and processes controlling the consolidation of FYI ridges through the infiltration and freezing of snow meltwater, however, are largely unknown. Furthermore, the scale of this phenomenon cannot be fully understood without a better understanding of the process. Nevertheless, the fact that we observed this phenomenon at two separate ridges and at multiple coring locations within the same ridge provides some indication that this process could be widespread across the Arctic and an important process in terms of FYI ridge consolidation and the progression into MYI ridges.

The higher macro-porosity of FYI ridges (i.e., presence of voids) compared to MYI ridges (i.e., absence of voids or less voids) has been hypothesized to result from meltwater filling the voids within a FYI ridge, which then refreezes as the ridge evolves into a MYI ridge (Richter-Menge and Cox, 1985). Here we provide first evidence that snow meltwater plays an important role in the consolidation of FYI ridges. Perhaps one surprising aspect of this finding is that the refreezing and consolidation occurs during the advanced summer melt period. The incorporation of snow meltwater within the ridge results in stronger ice, which could pose a higher risk than previously thought for shipping and offshore activities during the peak summer season. The meltwater incorporation and refreezing decreases the bulk salinity and increases consolidation. Subsequently, the ridge contains a greater mass of ice and higher density, requiring more thermal energy to melt. Thus, the snowmelt infiltration and ridge consolidation event we observed may result in increased survivability of FYI ridges during peak melt with important implications for sea ice mass balance on a pan-Arctic scale.

First-year ice ridges represent ecological hotspots (Hop and Pavlova, 2008; Lange et al., 2017b; Fernández-Méndez et al., 2018), which may serve as a refuge for ice-associated organisms with the ongoing shift in sea ice habitats (Gradinger et al., 2010). The suitability of FYI ridges as a habitat can be attributed, in large part, to the presence of large voids within the ridge keels, which offer additional habitable space and shelter from predators. Furthermore, these voids within FYI ridges enhance light scattering, consequently increasing the available light for photosynthetic organisms living within the ridge (Katlein et al., 2021). Snowmelt infiltration fills these voids and consolidates the ridge, which essentially reduces the habitable space, limits nutrient resupply, and further reduces the scattering of light, decreasing available light levels for organisms living within the ridge.

4. Summary and conclusions

Here, we have presented first evidence that snow meltwater has a significant contribution to Arctic FYI ridge consolidation, perhaps unexpectedly, during the peak of summer snow and ice melt. The oxygen isotopic signatures indicated a large snow contribution to ice mass within the two sampled ridges. We attributed this contribution to the infiltration of fresh snow meltwater into the voids in the ridge keel, either through percolation through the ridge or lateral infiltration to the ridge keel, which subsequently refroze as a result of the increased capacity of the ridge to absorb heat from the infiltrating meltwater without further melting and rapidly consolidating the ridge keel. However, the mass and energy budget of such a consolidation process, and the exact mechanism explaining the pathways of snow meltwater to the ridge keel need further investigation and are the topic of ongoing studies. The freshening and consolidation likely increased the strength of the FYI ridges during the summer melt season when sea ice is assumed to be weakest with implications for offshore and shipping activities. The snowmelt infiltration and consolidation process also has a positive impact

on sea ice mass balance at a time when ice is otherwise melting, and likely increases the survivability of FYI ridges. Lastly, the refreezing of the voids in the keel likely reduces light levels and the habitable space available for organisms within FYI ridges, which likely has negative ecological impacts as ridges have been identified as ecological hotspots.

Data accessibility statement

All sea ice and snow oxygen isotope and salinity data used in this study are published on PANGAEA (Lange et al., 2022a, 2022b) available online here: https://doi.org/10.1594/PANGAEA.943744 and https://doi.org/10.1594/PANGAEA.943746.

Acknowledgments

This work was carried out and data used in this manuscript was produced as part of the international Multidisciplinary drifting Observatory for the Study of the Arctic Climate (MOSAiC) with the tag MOSAiC20192020. We thank all persons involved in the expedition of the Research Vessel *Polarstern* (Alfred-Wegener-Institut Helmholtz-Zentrum für Polar- und Meeresforschung, 2017) during MOSAiC in 2019–2020 (AWI_PS122_00) as listed in Nixdorf et al. (2021). We gratefully acknowledge Ilkka Matero and Ian A. Raphael for support processing ice core samples onboard *Polarstern*. We thank the detailed and constructive feedback provided by the two reviewers.

Funding

This work was supported by the Norwegian Polar Institute's Arctic Ocean program and the Research Council of Norway through projects CAATEX (grant no. 280531) and HAVOC (grant no. 280292) and the European Union's Horizon 2020 research and innovation program project ARICE (EU grant no. 730965). DK was funded by the Research Council of Norway through the project The Nansen Legacy (grant no. 276730). AM and MS were funded through Swiss Polar Institute (grant SnowMOSAiC).

Competing interests

The authors declare that they have no conflict of interest.

Author contributions

Contributed to conception and design: BAL, ES, MAG.

Contributed to acquisition of data: BAL, ES, AM, JG, OM.

Contributed to analysis and interpretation of data: BAL, ES, AM, MS, KH, JG, OM, DVD, DK, CK, MAG.

Drafted and/or revised the article: BAL drafted the first version of the manuscript, and all authors contributed to writing and revisions.

Approved the submitted version for publication: All authors.

References

Alfred-Wegener-Institut Helmholtz-Zentrum für Polar- und Meeresforschung. 2017. Polar research and supply vessel POLARSTERN operated by the Alfred-Wegener-Institute. *Journal of Large-Scale Research Facilities* **3**. DOI: http://dx.doi.org/10.17815/jlsrf-3-163.

Cox, GFN, **Weeks, WF.** 1974. Salinity variations in sea ice. *Journal of Glaciology* **13**(67): 109–120. DOI: http://dx.doi.org/10.3189/S0022143000023418.

Eicken, H, **Krouse, HR**, **Perovich, DK.** 2002. Tracer studies of pathways and rates of meltwater transport through Arctic summer sea ice. *Journal of Geophysical Research* **107**(C10). DOI: http://dx.doi.org/10.1029/2000jc000583.

Fernández-Méndez, M, **Olsen, LM**, **Kauko, HM**, **Meyer, A**, **Rösel, A**, **Merkouriadi, I**, **Mundy, CJ**, **Ehn, JK**, **Johansson, AM**, **Wagner, PM**, **Ervik, Å**, **Sorrell, BK**, **Duarte, P**, **Wold, A**, **Hop, H**, **Assmy, P**. 2018. Algal hot spots in a changing Arctic Ocean: Sea-ice ridges and the snow-ice interface. *Frontiers in Marine Science* **5**(75). DOI: http://dx.doi.org/10.3389/fmars.2018.00075.

Gradinger, R, **Bluhm, B**, **Iken, K.** 2010. Arctic sea-ice ridges—Safe heavens for sea-ice fauna during periods of extreme ice melt? *Deep Sea Research Part II: Topical Studies in Oceanography* **57**(1–2): 86–95. DOI: http://dx.doi.org/10.1016/j.dsr2.2009.08.008.

Granskog, MA, **Rösel, A**, **Dodd, PA**, **Divine, D**, **Gerland, S**, **Martma, T**, **Leng, MJ.** 2017. Snow contribution to first-year and second-year Arctic sea ice mass balance north of Svalbard. *Journal of Geophysical Research: Oceans* **122**(3): 2539–2549. DOI: http://dx.doi.org/10.1002/2016jc012398.

Hansen, E, **Gerland, S**, **Granskog, MA**, **Pavlova, O**, **Renner, AHH**, **Haapala, J**, **Løyning, TB**, **Tschudi, M.** 2013. Thinning of Arctic sea ice observed in Fram Strait: 1990–2011. *Journal of Geophysical Research: Oceans* **118**(10): 5202–5221. DOI: http://dx.doi.org/10.1002/jgrc.20393.

Hop, H, **Pavlova, O.** 2008. Distribution and biomass transport of ice amphipods in drifting sea ice around Svalbard. *Deep Sea Research Part II: Topical Studies in Oceanography* **55**(20–21): 2292–2307. DOI: http://dx.doi.org/10.1016/j.dsr2.2008.05.023.

Høyland, KV. 2002. Consolidation of first-year sea ice ridges. *Journal of Geophysical Research* **107**(C6). DOI: http://dx.doi.org/10.1029/2000jc000526.

Itkin, P, **Hendricks, S**, **Webster, M**, **von Albedyll, L**, **Arndt, S**, **Divine, D**, **Jaggi, M**, **Oggier, M**, **Raphael, I**, **Ricker, R**, **Rohde, J**, **Schneebeli, M**, **Liston, GE.** 2023. Sea ice and snow characteristics from yearlong transects at the MOSAiC Central Observatory. *Elementa: Science of the Anthropocene* **11**(1). DOI: http://dx.doi.org/10.1525/elementa.2022.00048.

Itkin, P, **Spreen, G**, **Cheng, B**, **Doble, M**, **Girard-Ardhuin, F**, **Haapala, J**, **Hughes, N**, **Kaleschke, L**, **Nicolaus, M**, **Wilkinson, J.** 2017. Thin ice and storms: Sea ice deformation from buoy arrays deployed during N-ICE2015. *Journal of Geophysical Research: Oceans* **122**(6): 4661–4674. DOI: http://dx.doi.org/10.1002/2016jc012403.

Johnston, ME. 2017. Seasonal changes in the properties of first-year, second-year and multi-year ice. *Cold Regions Science and Technology* **141**: 36–53. DOI:

http://dx.doi.org/10.1016/j.coldregions.2017.05.006.

Katlein, C, **Langelier, JP**, **Ouellet, A**, **Lévesque-Desrosiers, F**, **Hisette, Q**, **Lange, BA**, **Lambert-Girard, S**, **Babin, M**, **Thibault, S.** 2021. The three-dimensional light field within sea ice ridges. *Geophysical Research Letters* **48**(11). DOI: http://dx.doi.org/10.1029/2021gl093207.

Kopec, BG, **Feng, X**, **Michel, FA**, **Posmentier, ES.** 2016. Influence of sea ice on Arctic precipitation. *Proceedings of the National Academy of Sciences* **113**(1): 46–51. DOI: http://dx.doi.org/10.1073/pnas.1504633113.

Krumpen, T, **von Albedyll, L**, **Goessling, HF**, **Hendricks, S**, **Juhls, B**, **Spreen, G**, **Willmes, S**, **Belter, HJ**, **Dethloff, K**, **Haas, C**, **Kaleschke, L**, **Katlein, C**, **Tian-Kunze, X**, **Ricker, R**, **Rostosky, P**, **Rückert, J**, **Singha, S**, **Sokolova, J.** 2021. MOSAiC drift expedition from October 2019 to July 2020: Sea ice conditions from space and comparison with previous years. *The Cryosphere* **15**(8): 3897–3920.

Kwok, R. 2018. Arctic sea ice thickness, volume, and multiyear ice coverage: Losses and coupled variability (1958–2018). *Environmental Research Letters* **13**(10). DOI: http://dx.doi.org/10.1088/1748-9326/aae3ec.

Lange, BA, **Flores, H**, **Michel, C**, **Beckers, JF**, **Bublitz, A**, **Casey, JA**, **Castellani, G**, **Hatam, I**, **Reppchen, A**, **Rudolph, SA**, **Haas, C.** 2017a. Pan-Arctic sea ice-algal chl *a* biomass and suitable habitat are largely underestimated for multi-year ice. *Global Change Biology* **23**(11): 4581–4597. DOI: http://dx.doi.org/10.1111/gcb.13742.

Lange, BA, **Haas, C**, **Charette, J**, **Katlein, C**, **Campbell, K**, **Duerksen, S**, **Coupel, P**, **Anhaus, P**, **Jutila, A**, **Tremblay, POG**, **Carlyle, CG**, **Michel, C.** 2019. Contrasting ice algae and snow-dependent irradiance relationships between first-year and multi-year sea ice. *Geophysical Research Letters* **46**(19): 10834–10843.

Lange, BA, **Haas, C**, **Mucci, A**, **Beckers, JF**, **Casey, JA**, **Duerksen, S**, **Granskog, MA**, **Hatam, I**, **Niemi, A**, **Reppchen, A**, **Michel, C.** 2021. Contribution of snow to Arctic first-year and multi-year sea ice mass balance within the last ice area. *Journal of Geophysical Research: Oceans* **126**(5): e2020JC016971. DOI: http://dx.doi.org/10.1029/2020jc016971.

Lange, BA, **Katlein, C**, **Castellani, G**, **Fernández-Méndez, M**, **Nicolaus, M**, **Peeken, I**, **Flores, H.** 2017b. Characterizing spatial variability of ice algal chlorophyll *a* and net primary production between sea ice habitats using horizontal profiling platforms. *Frontiers in Marine Science: Ocean Observation* **4**: 349. DOI: http://dx.doi.org/10.3389/fmars.2017.00349.

Leppäranta, M, **Lensu, M**, **Kosloff, P**, **Veitch, B.** 1995. The life story of a first-year sea ice ridge. *Cold Regions Science and Technology* **23**(3): 279–290. DOI: http://dx.doi.org/10.1016/0165-232X(94)00019-T.

Liston, GE, **Polashenski, C**, **Rösel, A**, **Itkin, P**, **King, J**, **Merkouriadi, I**, **Haapala, J.** 2018. A distributed snow-evolution model for sea-ice applications (SnowModel). *Journal of Geophysical Research: Oceans* **123**(5): 3786–3810. DOI: http://dx.doi.org/10.1002/2017jc013706.

Marchenko, A. 2008. Thermodynamic consolidation and melting of sea ice ridges. *Cold Regions Science and Technology* **52**(3): 278–301. DOI: http://dx.doi.org/10.1016/j.coldregions.2007.06.008.

Nicolaus, M, **Perovich, DK**, **Spreen, G**, **Granskog, MA**, **von Albedyll, L**, **Angelopoulos, M**, **Anhaus, P**, **Arndt, S**, **Belter, HJ**, **Bessonov, V**, **Birnbaum, G**, **Brauchle, J**, **Calmer, R**, **Cardellach, E**, **Cheng, B**, **Clemens-Sewall, D**, **Dadic, R**, **Damm, E**, **de Boer, G**, **Demir, O**, **Dethloff, K**, **Divine, DV**, **Fong, AA**, **Fons, S**, **Frey, MM**, **Fuchs, N**, **Gabarró, C**, **Gerland, S**, **Goessling, HF**, **Gradinger, R**, **Haapala, J**, **Haas, C**, **Hamilton, J**, **Hannula, H-R**, **Hendricks, S**, **Herber, A**, **Heuzé, C**, **Hoppmann, M**, **Høyland, KV**, **Huntemann, M**, **Hutchings, JK**, **Hwang, B**, **Itkin, P**, **Jacobi, H-W**, **Jaggi, M**, **Jutila, A**, **Kaleschke, L**, **Katlein, C**, **Kolabutin, N**, **Krampe, D**, **Kristensen, SS**, **Krumpen, T**, **Kurtz, N**, **Lampert, A**, **Lange, BA**, **Lei, R**, **Light, B**, **Linhardt, F**, **Liston, GE**, **Loose, B**, **Macfarlane, AR**, **Mahmud, M**, **Matero, IO**, **Maus, S**, **Morgenstern, A**, **Naderpour, R**, **Nandan, V**, **Niubom, A**, **Oggier, M**, **Oppelt, N**, **Pätzold, F**, **Perron, C**, **Petrovsky, T**, **Pirazzini, R**, **Polashenski, C**, **Rabe, B**, **Raphael, IA**, **Regnery, J**, **Rex, M**, **Ricker, R**, **Riemann-Campe, K**, **Rinke, A**, **Rohde, J**, **Salganik, E**, **Scharien, RK**, **Schiller, M**, **Schneebeli, M**, **Semmling, M**, **Shimanchuk, E**, **Shupe, MD**, **Smith, MM**, **Smolyanitsky, V**, **Sokolov, V**, **Stanton, T**, **Stroeve, J**, **Thielke, L**, **Timofeeva, A**, **Tonboe, RT**, **Tavri, A**, **Tsamados, M**, **Wagner, DN**, **Watkins, D**, **Webster, M**, **Wendisch, M**. 2022. Overview of the MOSAiC expedition: Snow and sea ice. *Elementa: Science of the Anthropocene* **10**(1). DOI: http://dx.doi.org/10.1525/elementa.2021.000046.

Nixdorf, U, **Dethloff, K**, **Rex, M**, **Shupe, M**, **Sommerfeld, A**, **Perovich, DK**, **Nicolaus, M**, **Heuzé, C**, **Rabe, B**, **Loose, B**, **Damm, E**, **Gradinger, R**, **Fong, A**, **Maslowski, W**, **Rinke, A**, **Kwok, R**, **Spreen, G**, **Wendisch, M**, **Herber, A**, **Boetius, A.** 2021. MOSAiC extended acknowledgement. Zenodo. DOI: http://dx.doi.org/10.5281/zenodo.5541624.

Parnell, AC, **Phillips, DL**, **Bearhop, S**, **Semmens, BX**, **Ward, EJ**, **Moore, JW**, **Jackson, AL**, **Grey, J**, **Kelly, DJ**, **Inger, R**. 2013. Bayesian stable isotope mixing models. *Environmetrics* **24**(6): 387–399. DOI: http://dx.doi.org/10.1002/env.2221.

Pörtner, HO, **Roberts, DC**, **Masson-Delmotte, V**, **Zhai, P**, **Tignor, M**, **Poloczanska, E**, **Mintenbeck, K**, **Alegría, A**, **Nicolai, M**, **Okem, A**, **Petzold, J**, **Rama, B**, **Weyer, NM**. 2019. *IPCC Special Report on the Ocean and Cryosphere in a Changing Climate*. Geneva, Switzerland: IPCC.

Rampal, P, **Weiss, J**, **Dubois, C**, **Campin, JM**. 2011. IPCC climate models do not capture Arctic sea ice drift acceleration: Consequences in terms of projected sea ice thinning and decline. *Journal of Geophysical*

Research **116**(C8): C00D07. DOI: http://dx.doi.org/10.1029/2011JC007110.

R-Development-Core-Team. 2018. *v. 3.5.0. R: A Language and Environment for Statistical Computing*. Vienna, Austria: R Foundation for Statistical Computing.

Richter-Menge, JA, **Cox, GFN**. 1985. Structure, salinity and density of multi-year sea ice pressure ridges. *Journal of Energy Resources Technology* **107**(4): 493–497. DOI: http://dx.doi.org/10.1115/1.3231224.

Salganik, E, **Katlein, C**, **Lange, BA**, **Matero, I**, **Lei, R**, **Fong, AA**, **Fons, SW**, **Divine, D**, **Oggier, M**, **Castellani, G**, **Bozzato, D**, **Chamberlain, EJ**, **Hoppe, CJM**, **Müller, O**, **Gardner, J**, **Rinke, A**, **Pereira, PS**, **Ulfsbo, A**, **Marsay, C**, **Webster, MA**, **Maus, S**, **Høyland, KV**, **Granskog, MA**. 2023. Temporal evolution of under-ice meltwater layers and false bottoms and their impact on summer Arctic sea ice mass balance. *Elementa: Science of the Anthropocene* **11**(1). DOI: http://dx.doi.org/10.1525/elementa.2022.00035.

Shestov, A, **Høyland, K**, **Ekeberg, O**. 2012. Morphology and physical properties of old sea ice in the Fram Strait 2006–2011, in *Proceedings of the 21th International Symposium on Ice (IAHR)*. Available at https://trid.trb.org/view/1353019.

Shestov, A, **Høyland, K**, **Ervik, Å**. 2018. Decay phase thermodynamics of ice ridges in the Arctic Ocean. *Cold Regions Science and Technology* **152**: 23–34. DOI: http://dx.doi.org/10.1016/j.coldregions.2018.04.005.

Shestov, AS, **Marchenko, AV**. 2016a. The consolidation of saline ice blocks in water of varying freezing points: Laboratory experiments and computer simulations. *Cold Regions Science and Technology* **122**: 71–79. DOI: http://dx.doi.org/10.1016/j.coldregions.2015.11.008.

Shestov, AS, **Marchenko, AV**. 2016b. Thermodynamic consolidation of ice ridge keels in water at varying freezing points. *Cold Regions Science and Technology* **121**: 1–10. DOI: http://dx.doi.org/10.1016/j.coldregions.2015.09.015.

Smith, MM, **von Albedyll, L**, **Raphael, IA**, **Lange, BA**, **Matero, I**, **Salganik, E**, **Webster, MA**, **Granskog, MA**, **Fong, A**, **Lei, RB**, **Light, B**. 2022. Quantifying false bottoms and under-ice meltwater layers beneath Arctic summer sea ice with fine-scale observations. *Elementa: Science of the Anthropocene* **10**(1). DOI: http://dx.doi.org/10.1525/elementa.2021.000116.

Stock, BC, **Jackson, AL**, **Ward, EJ**, **Parnell, AC**, **Phillips, DL**, **Semmens, BX**. 2018. Analyzing mixing systems using a new generation of Bayesian tracer mixing models. *PeerJ* **6**: e5096. DOI: http://dx.doi.org/10.7717/peerj.5096.

Stroeve, J, **Notz, D**. 2018. Changing state of Arctic sea ice across all seasons. *Environmental Research Letters* **13**(10). DOI: http://dx.doi.org/10.1088/1748-9326/aade56.

Tian, L, **Gao, Y**, **Ackley, SF**, **Stammerjohn, S**, **Maksym, T**, **Weissling, B**. 2018. Stable isotope clues to the formation and evolution of refrozen melt ponds on Arctic sea ice. *Journal of Geophysical Research: Oceans* **123**(12): 8887–8901. DOI: http://dx.doi.org/10.1029/2018jc013797.

Timco, GW, **Burden, RP**. 1997. An analysis of the shapes of sea ice ridges. *Cold Regions Science and Technology* **25**(1): 65–77. DOI: http://dx.doi.org/10.1016/S0165-232X(96)00017-1.

Wadhams, P, **Toberg, N**. 2012. Changing characteristics of Arctic pressure ridges. *Polar Science* **6**(1): 71–77.

Wright, BD, **Timco, GW**. 2001. First-year ridge interaction with the Molikpaq in the Beaufort Sea. *Cold Regions Science and Technology* **32**(1): 27–44. DOI: http://dx.doi.org/10.1016/S0165-232X(01)00021-0.

How to cite this article: Lange, BA, Salganik, E, Macfarlane, A, Schneebeli, M, Høyland, K, Gardner, J, Müller, O, Divine, DV, Kohlbach, D, Katlein, C, Granskog, MA. 2023. Snowmelt contribution to Arctic first-year ice ridge mass balance and rapid consolidation during summer melt. *Elementa: Science of the Anthropocene* 11(1). DOI: https://doi.org/10.1525/elementa.2022.00037

Domain Editor-in-Chief: Jody W. Deming, University of Washington, Seattle, WA, USA

Associate Editor: Marcel Nicolaus, Alfred-Wegener-Institut Helmholtz-Zentrum für Polar- und Meeresforschung, Bremerhaven, Germany

Knowledge Domain: Ocean Science

Part of an Elementa Special Feature: The Multidisciplinary Drifting Observatory for the Study of Arctic Climate (MOSAiC)

Published: May 29, 2023 **Accepted:** April 19, 2023 **Submitted:** March 03, 2022

ELEMENTA Science of the Anthropocene

Elem Sci Anth is a peer-reviewed open access journal published by University of California Press.

OPEN ACCESS